Nanoscale Res Lett (2009) 4:307–312
DOI 10.1007/s11671-008-9243-0

NANO EXPRESS

Thermally Induced Nano-Structural and Optical Changes of nc-Si:H Deposited by Hot-Wire CVD

C. J. Arendse · G. F. Malgas · T. F. G. Muller · D. Knoesen · C. J. Oliphant · D. E. Motaung · S. Halindintwali · B. W. Mwakikunga

Received: 28 October 2008 / Accepted: 30 December 2008 / Published online: 21 January 2009

Abstract We report on the thermally induced changes of the nano-structural and optical properties of hydrogenated nanocrystalline silicon in the temperature range 200–700 °C. The as-deposited sample has a high crystalline volume fraction of 53% with an average crystallite size of ~3.9 nm, where 66% of the total hydrogen is bonded as ≡Si–H monohydrides on the nano-crystallite surface. A growth in the native crystallite size and crystalline volume fraction occurs at annealing temperatures ≥400 °C, where hydrogen is initially removed from the crystallite grain boundaries followed by its removal from the amorphous network. The nucleation of smaller nano-crystallites at higher temperatures accounts for the enhanced porous structure and the increase in the optical band gap and average gap.

C. J. Arendse (✉) · G. F. Malgas (✉) ·
C. J. Oliphant · D. E. Motaung · B. W. Mwakikunga
CSIR National Centre for Nano-Structured Materials,
P.O. Box 395, Pretoria 0001, South Africa
e-mail: CArendse01@gmail.com

G. F. Malgas
e-mail: GMalgas@csir.co.za

C. J. Arendse · T. F. G. Muller · D. Knoesen ·
C. J. Oliphant · D. E. Motaung · S. Halindintwali
Department of Physics, University of the Western Cape,
Private Bag X17, Bellville 7535, South Africa

B. W. Mwakikunga
School of Physics, University of the Witwatersrand,
Private Bag 3, P.O. Wits, Johannesburg 2050, South Africa

B. W. Mwakikunga
Department of Physics, University of Malawi, The Polytechnic,
Private Bag 303, Blantyre, Malawi

Keywords Hot-wire CVD · Quantum size effects · Nano-crystallite · Optical band gap

Introduction

Hydrogenated nanocrystalline silicon (nc-Si:H) has been the subject of intense scientific and technological interest over the past decade, mainly due to its reduced photo-induced degradation [1], efficient visible photoluminescence [2], tailored optical band gap [3], increased conductivity and greater doping efficiency [4]. It has been highlighted that these unique features are a direct cause of the quantum size effects of the silicon nano-crystallites. These improvements make nc-Si:H a potential candidate for application in photovoltaic and opto-electronic devices [5, 6].

The hot-wire chemical vapour deposition (HWCVD) technique, based on the catalytic decomposition of the precursor gasses by a heated transition metal filament, has been established as a viable deposition technique for nc-Si:H thin films [6, 7]. The structural and opto-electronic properties of the thin films are dependent on the deposition parameters, of which the hydrogen dilution and substrate temperature are the most crucial. It has been established that the etching effect of atomic hydrogen, created by the catalytic decomposition of H_2, is responsible for the termination of weak Si–Si bonds from the surface and sub-surface regions and that the nucleation of the nano-crystallites are improved by increasing the hydrogen dilution [7–10]. It has also been reported that the hydrogen dilution during deposition determines the concentration and the distribution of hydrogen in nc-Si:H, which is closely related to the nano-structural features; i.e. crystallite size and crystalline volume fraction [11–14]. These nano-structural

features eventually determine the optical properties of the material. In particular, the quantum size effects of the Si nano-crystallites and the hydrogen concentration have a strong correlation with the optical band gap [15, 16].

An investigation into the role of hydrogen in nc-Si:H is therefore crucial for the understanding of its relation to the nano-structure and the optical properties. In this contribution, we investigate the effects of the hydrogen concentration and bonding configuration in nc-Si:H deposited by HWCVD on the nano-structural features and the optical properties. The hydrogen concentration and bonding configuration were controlled by post-deposition isochronal annealing.

Experimental

The nc-Si:H thin film was deposited by the HWCVD process simultaneously on single-side polished ⟨100⟩ crystalline silicon and Corning 7059 glass substrates, using a mixture of 4 sccm SiH_4 and 26 sccm H_2 decomposed by seven parallel tungsten filaments, 15 cm apart and 36 cm away from the substrates. A detailed description of the experimental set-up is given elsewhere [17, 18]. The filament temperature, substrate temperature and deposition pressure were fixed at 1600 °C, 420 °C and 60 μbar, respectively. The as-deposited nc-Si:H thin film was $\sim$1140 nm-thick, as measured using a Veeco® profilometer.

Subsequent annealing was performed under high-purity, flowing N_2 gas in a tube furnace at annealing temperatures (T_A) ranging from 200 to 700 °C in 100 °C increments. The N_2 flow rate, heating rate and dwell time for all temperatures amounted to 300 sccm, 10 °C/min and 30 min, respectively. After each annealing temperature, the thin film was allowed to cool to room temperature in the tube furnace, while maintaining the N_2 flow rate. Thereafter the required analytical techniques were performed.

Fourier transform infrared (FTIR) absorption spectra were collected in transmission geometry from 400 to 4000 cm^{-1} with a spectral resolution of 1 cm^{-1}, using a Perkin-Elmer Spectrum 100 FTIR spectrophotometer. The structural properties were investigated using a Jobin-Yvon HR800 micro-Raman spectrometer in backscattering geometry at room temperature. The Raman spectra were collected in the region 100–1000 cm^{-1} with a spectral resolution of 0.4 cm^{-1}, using an excitation wavelength of 514.5 nm. X-ray diffraction (XRD) spectra were collected in reflection geometry at 2θ-values ranging from 10 to 90° with a step size of 0.02°, using a Phillips PW 1830 X-ray powder diffractometer operating at 45 kV and 40 mA. Copper $K\alpha_1$ radiation with a wavelength of 1.5406 Å was used as the X-ray source. Optical transmission spectra were measured from 200 to 900 nm with a spectral resolution of 1 nm, using a Perkin-Elmer LAMDA 750S UV/VIS spectrophotometer.

Results and Discussion

Nano-Structural Properties

FTIR spectroscopy is the established analytical technique of choice to probe the silicon–hydrogen bonding configurations and to calculate the hydrogen concentration in nc-Si:H and related material. The FTIR absorption spectrum of the sample in the as-deposited state is shown in Fig. 1. The strong absorption bands in the region 920–1250 cm^{-1} is associated with the asymmetric Si–O–Si stretching vibration [19], whereas the peak centred around 2250 cm^{-1} is assigned to the H–SiO_3 vibration [20]. This is indicative of an oxidation effect caused by its porous-like microstructure, which is a typical feature for nc-Si:H thin films [9, 21]. The enhanced absorption band centred around 640 cm^{-1} is attributed to the rocking vibrations of all bonding configurations of Si–H_x [22]. The absorption bands in the region 1900–2150 cm^{-1} is a result of the convolution of several absorption bands associated with the stretching vibrations of Si–H_x in different configurations. This is illustrated in the insert of Fig. 1, where the absorption spectrum is decomposed into three Gaussian components. The absorption peaks centred around 1985 cm^{-1} and 2090 cm^{-1} are assigned to the stretching vibrations of $\equiv$Si–H monohydrides in the amorphous network (isolated) and on the surface of the Si nano-crystallites (clustered), respectively, [21, 23]. The weak absorption band centred at $\sim$2130 cm^{-1} is assigned to the

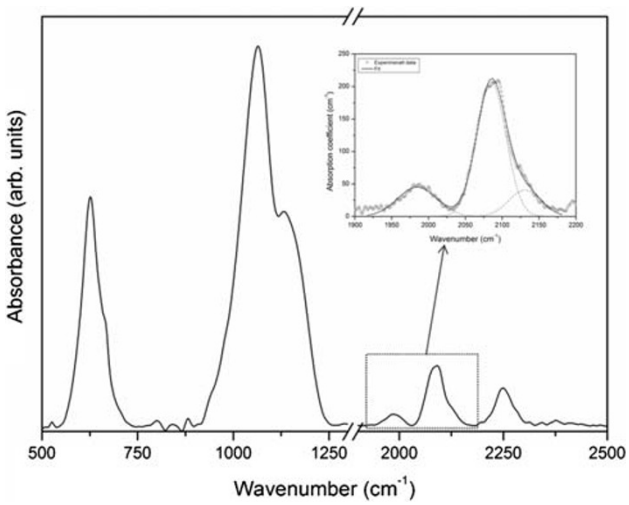

Fig. 1 FTIR absorption spectrum of the as-deposited sample and the deconvolution of the stretching vibrations (insert)

existence of $(=Si=H_2)_n$ polyhydride complexes on Si nano-crystallite grain boundaries [24, 25].

To quantify the fraction of H bonded on the surface of nano-crystallites in nc-Si:H, we define a structure factor, $R_s = I_{2090}/[I_{1985} + I_{2090} + I_{2130}]$, where I denotes that integrated intensity of each decomposed peak. The total bonded hydrogen concentration (C_H) was estimated from the integrated absorption of the 640 cm^{-1} rocking mode using previous reported procedures [26, 27]. In the as-deposited state, C_H amounts to $\sim$2 at.%, characteristic for nc-Si:H deposited with high hydrogen dilution [16, 28], where $\sim$66% thereof is bonded on the surface of the nano-crystallites. We propose that this relatively high value for R_s is indicative of a high crystalline volume fraction.

Figure 2 shows the plots of the hydrogen concentration and the structure factor as a function of annealing temperature. The hydrogen concentration and structure factor are relatively constant at temperatures below 400 °C, demonstrating that the nano-structure is stable in this temperature regime. After annealing at 400 °C most of the $(=Si=H_2)_n$ polyhydride bonds on the grain boundaries of the Si nano-crystallites have been terminated and consequently results in an increase in the structure factor. Annealing at higher temperatures induce a significant decrease in C_H, coupled with an increase in R_s. These changes are caused by the preferential termination of the isolated $\equiv$Si–H bonds in the amorphous network. We propose that the instability induced at $T_A \geq 400$ °C is related to the growth of the native nano-crystallites and to the nucleation of nano-crystallites in the amorphous network, thereby resulting in an increase in the crystalline volume fraction. It should be noted that no Si–H_x absorption peaks were identified after annealing at 700 °C.

Raman spectroscopy provides direct nano-structural information quantitatively related to the average nano-crystallite

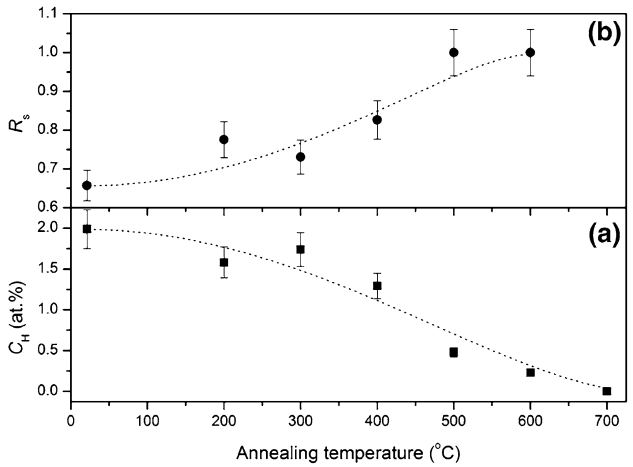

Fig. 2 **a** Hydrogen concentration and **b** the structure factor as a function of annealing temperature

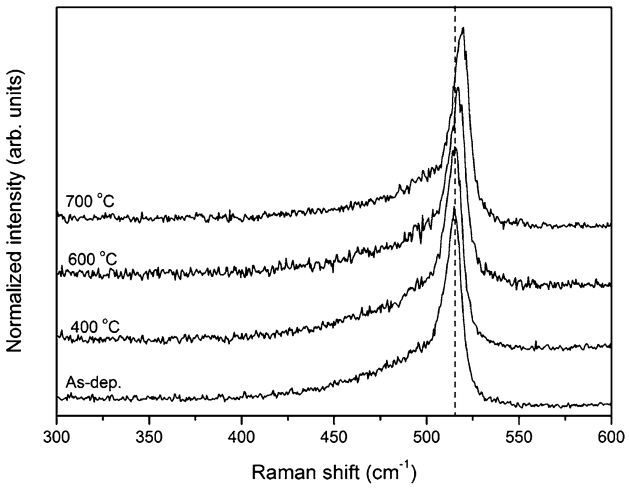

Fig. 3 Raman spectra of the sample in the as-deposited state and after annealing at specific temperatures

size and the crystalline volume fraction in nc-Si:H. Figure 3 shows the Raman spectra of the sample in the as-deposited state and after annealing at specific temperatures. All spectra display the following main features: (i) a sharp peak centred around 515 cm^{-1}, associated with the transverse optic (TO) mode of the nc-Si phase; (ii) the broad shoulder centred around 480 cm^{-1}, due to the TO-mode of the amorphous silicon (a-Si) phase; and (iii) a smaller shoulder around 505 cm^{-1}, corresponding to the distribution of crystalline grain boundaries in the sample.

The crystalline volume fraction, $f_c = [A_{505} + A_{515}]/[A_{480} + A_{505} + A_{515}]$, can be estimated from the integrated areas of the afore-mentioned deconvoluted Gaussian peaks [29]. The crystallite size is empirically calculated from $d_{Raman} = 2\pi\sqrt{B/\Delta\omega}$, where $\Delta\omega$ is the shift of the 515 cm^{-1} peak relative to the c-Si peak at 520 cm^{-1} and $B = 2.0$ cm^{-2} [30]. The quantitative Raman results are summarized in Table 1. In the as-deposited state, the average crystallite size and the crystalline volume fraction amounts to about 3.9 nm and 53%, respectively, and remain relatively constant after annealing at 300 °C. These observations reiterate that the nano-structure of the sample remains stable at temperatures below 400 °C. A blue shift

Table 1 Crystallite size, crystalline volume fraction and optical properties after specific annealing temperatures

T_A (°C)	d_{Raman} (nm)	f_c (%)	n_o	E_M (eV)	E_{04} (eV)
As-dep	3.9	53	2.750	3.11	1.88
400	4.7	57	2.758	3.05	1.87
600	5.2	59	2.668	3.03	1.84
700	8.4	64	2.651	3.10	1.87

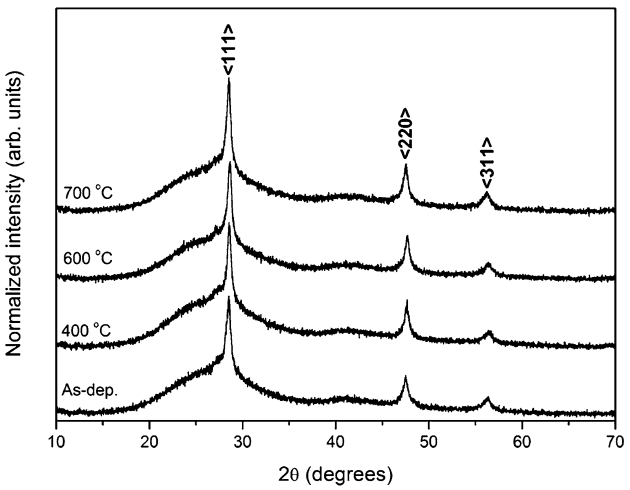

Fig. 4 XRD spectra of the sample in the as-deposited state and after annealing at specific temperatures

of the nc-Si TO-peak, accompanied with a reduction in the intensity of the a-Si TO-peak is observed at annealing temperatures $\geq$400 °C, indicative of an increase in the crystallite size and the crystalline volume fraction, respectively, and supports the claims based on the FTIR results.

XRD was employed as a complimentary method to qualitatively probe the changes in the crystallinity as a function of annealing temperature (see Fig. 4). Three preferential orientations in the $\langle 111 \rangle$, $\langle 200 \rangle$ and $\langle 311 \rangle$ directions are observed. The crystallite size in the as-deposited state, estimated from the full-width-half-maximum (FWHM) of the (111)-peak, amounts to $\sim$19.5 nm [31]. A narrowing in the FWHM of the (111)-peak, accompanied with an increase in its intensity is observed with an increase in annealing temperature. This confirms the increase of the crystallite size and crystalline volume fraction, as probed by Raman spectroscopy.

The thermally induced nano-structural changes of the nc-Si:H thin film can be interpreted as follows, based on the variation of the Si–H_x bonding and the crystalline character. In the as-deposited state the crystalline volume fraction is relatively large and therefore the majority of H is bonded to the surface of the nano-crystallites. The nano-structural properties are stable at temperatures below 400 °C, attributed to its large crystalline volume fraction. An initial increase in the native crystallite size is observed after annealing at 400 °C, resulting in the removal of hydrogen from the grain boundaries. It is also feasible that smaller crystallites have coalesced into larger crystallites. At higher temperatures, hydrogen is removed preferentially from the amorphous phase, indicative of the nucleation of smaller nano-crystallites of size <3 nm in the amorphous network [32], undetected by Raman spectroscopy and XRD.

Optical Properties

The optical properties were determined from UV–visible transmission measurements performed on the thin film deposited on the Corning 7059 glass substrate, using the method proposed by Swanepoel [33, 34]. The thickness of the as-deposited sample was calculated to be $\sim$1180 nm, which concurs to that measured by profilometry. The refractive index $n(v)$ of a material is an important optical parameter, since it is directly proportional to density [35]. Figure 5 shows the spectral dependence of the calculated refractive index for the sample in the as-deposited state and after annealing at specific temperatures. A slight increase in the refractive index is observed after annealing at 400 °C, followed by a decrease at higher temperatures. The initial increase can be ascribed to the increase in the native crystallite size and possibly due to the coalescence of smaller nano-crystallites. Furthermore, the presence of $(=Si=H_2)_n$ complexes in the as-deposited state is indicative of a disordered, porous material and the removal thereof after 400 °C would therefore result in a more compact material. The subsequent decrease of the refractive index at higher temperatures is attributed to a more porous structure, possibly caused by the nucleation of smaller nano-crystallites in the amorphous network. Similar trends in the refractive index at zero photon energy (n_o) are observed (see Table 1).

Detailed analysis of the refractive index spectra were performed using the model suggested by Wemple et al. [36]. At energies below than of the optical band gap, the refractive index is related to the square of the photon energy $(hv)^2$ by:

$$n^2(v) = 1 + \frac{E_M E_D}{E_M^2 - (hv)^2} \quad (1)$$

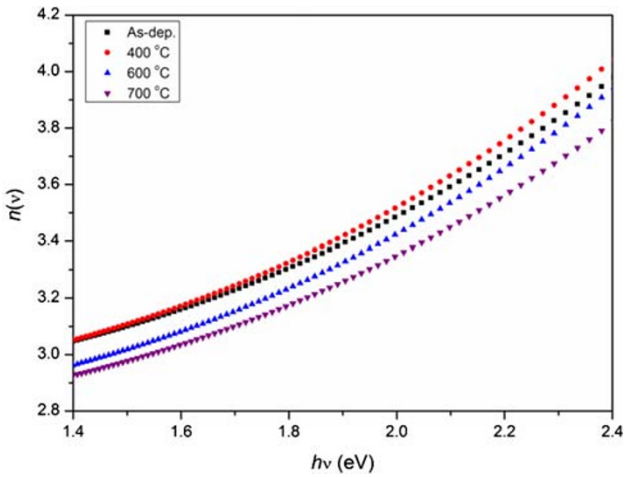

Fig. 5 Refractive index spectra of the sample in the as-deposited state and after annealing at specific temperatures

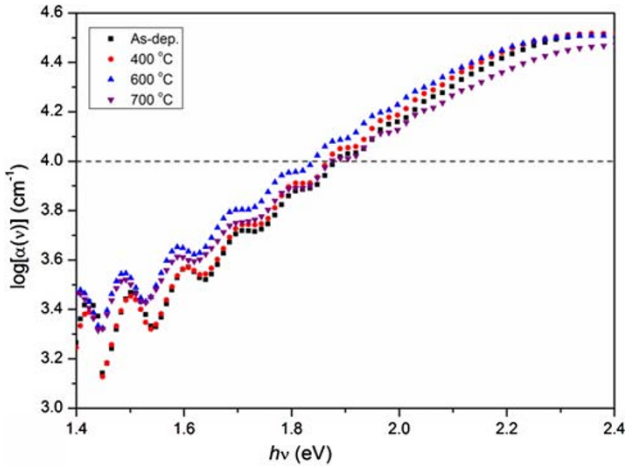

Fig. 6 Absorption coefficient spectra of the sample in the as-deposited state and after annealing at specific temperatures

where E_M and E_D is the average gap and dispersion energy, respectively. The plot of $1/[n^2(v)\text{-}1]$ versus $(hv)^2$ allows for the determination of E_M, E_D and n_o. The extrapolated results of n_o and E_M, calculated from the linear fit through the data, are listed in Table 1.

The spectral dependence of the absorption coefficient $\alpha(v)$ for the sample in the as-deposited state and after annealing at specific temperatures is depicted in Fig. 6. The optical band gap, referred to as E_{04}, is defined as the photon energy where $\alpha(v) = 10^4$ cm^{-1}, and the values are reported in Table 1. A red shift in E_{04} is observed for $T_A \leq 600$ °C followed by an unexpected blue shift after annealing at 700 °C. It is established that the optical band gap of hydrogenated amorphous silicon (a-Si:H) deposited by HWCVD and PECVD increases with an increase in the hydrogen concentration [7, 37]. It should be noted that the optical band gap for the sample in the as-deposited state is larger than that of a-Si:H with similar C_H values. This discrepancy is due to the presence of nano-crystallites in the amorphous network, which lowers the absorption in nc-Si:H and shifts the optical band gap towards higher energies [15, 16]. The quantum size effect size also predicts that an increase in crystallite size is associated with a decrease in the optical band gap. The initial decrease in E_{04} after 400 °C is due to the combined effect of the decreased C_H and the growth in the crystallite size. After annealing at 600 °C the initial hydrogen concentration has decreased by $\sim$90% with about the same incremental increase in the crystallite size as at 400 °C, and therefore a more notable decrease in E_{04} is expected. However, a minute 0.03 eV decrease in E_{04} is observed and is attributed to the nucleation of smaller nano-crystallites in the amorphous network, which explains the competing increasing effect on E_{04}. After annealing at 700 °C, where no hydrogen was detected by FTIR spectroscopy, this effect is more pronounced in that an increase in the optical band gap is observed.

The optical band gap and the average gap (E_M) have similar behaviours with respect to annealing temperature, thereby implying that the growth of the native nano-crystallites and the nucleation of smaller crystallites in the amorphous network have similar effects on the band edges and on the conduction and valence bands. Therefore, the average gap can be used to describe the thermal induced changes in the optical properties of nc-Si:H.

Conclusion

The effect of isochronal annealing on the nano-structural and optical properties of nc-Si:H, with the emphasis on its relation to the hydrogen distribution and concentration, was investigated. Initial changes in the nano-structure are observed after annealing at 400 °C, as evident by termination of $(=Si=H_2)_n$ polyhydrides from the grain boundaries caused by the growth of the native nano-crystallites. At higher temperatures, a further increase in the native nano-crystallite size and the crystalline volume fraction is observed, accompanied with the nucleation of smaller nano-crystallites and the subsequent removal of hydrogen from the amorphous network. At temperatures $\geq$600 °C the nucleation of the smaller nano-crystallites results in a porous material with an increased optical band gap and average gap, explained by the quantum size effect.

Acknowledgements The authors acknowledge the financial assistance of the Department of Science and Technology, the National Research Foundation and the Council for Scientific and Industrial Research (Project no: HGERA2S) of South Africa.

References

1. V. Shah, J. Meier, E. Vallat-Sauvain, N. Wyrsch, U. Kroll, C. Droz, U. Graf, Sol. Energy Mater. Sol. Cells **78**, 469 (2003). doi:10.1016/S0927-0248(02)00448-8
2. H. Takagi, H. Ogawa, Y. Yamazabi, A. Ishizaki, T. Nakakiri, Appl. Phys. Lett. **56**, 2379 (1990). doi:10.1063/1.102921
3. J. Kitao, H. Harada, N. Yoshida, Y. Kasuya, M. Nishio, T. Sakamoto, T. Itoh, S. Nonomura, Sol. Energy Mater. Sol. Cells **66**, 245 (2001). doi:10.1016/S0927-0248(00)00180-X
4. R. Saleh, N.H. Nickel, Thin Solid Films **427**, 266 (2003). doi:10.1016/S0040-6090(02)01203-8
5. S. Guha, J. Yang, D.L. Williamson, Y. Lubianiker, J.D. Cohen, A.H. Mahan, Appl. Phys. Lett. **74**, 1860 (1999). doi:10.1063/1.123693
6. R.E.I. Schropp, H. Li, R.H. Franken, J.K. Rath, C.H.M. van der Werf, J.W.A. Schüttauf, R.L. Stolk, Thin Solid Films **516**, 6818 (2008). doi:10.1016/j.tsf.2007.12.089
7. K.F. Feenstra, R.E.I. Schropp, W.F. van der Weg, J. Appl. Phys. **85**, 6843 (1999). doi:10.1063/1.370202
8. P. Brogueira, J.P. Conde, S. Arekat, V. Chu, J. Appl. Phys. **79**, 8748 (1996). doi:10.1063/1.362501

9. S. Halindintwali, D. Knoesen, R. Swanepoel, B.A. Julies, C. Arendse, T. Muller, C.C. Theron, A. Gordijn, P.C.P. Bronsveld, J.K. Rath, R.E.I. Schropp, Thin Solid Films **515**, 8040 (2007). doi:10.1016/j.tsf.2007.03.051
10. S.K. Kim, K.C. Park, J. Jang, J. Appl. Phys. **77**, 5115 (1995). doi:10.1063/1.359554
11. H. Li, R.H. Franken, R.L. Stolk, C.H.M. van der Werf, J.K. Rath, R.E.I. Schropp, J. Non-Cryst. Solids **354**, 2087 (2008). doi:10.1016/j.jnoncrysol.2007.10.046
12. S. Zhang, X. Liao, Y. Xu, R. Martins, E. Fortunato, G. Kong, J. Non-Cryst. Solids **338–340**, 188 (2004)
13. J.-H. Shim, Im Seongil, N.-H. Cho, Appl. Surf. Sci. **234**, 268 (2004). doi:10.1016/j.apsusc.2004.05.073
14. R. Amrani, D. Benlekehal, R. Baghdad, D. Senouci, A. Zeinert, K. Zellama, L. Chahed, J.D. Sib, Y. Bouizem, J. Non-Cryst. Solids **354**, 2291 (2008). doi:10.1016/j.jnoncrysol.2007.10.044
15. A.M. Ali, S. Hasegawa, Thin Solid Films **437**, 68 (2003). doi:10.1016/S0040-6090(03)00688-6
16. A.M. Funde, N.A. Bakr, D.K. Kamble, R.R. Hawaldar, D.P. Amalnerkar, S.R. Jadkar, Sol. Energy Mater. Sol. Cells **92**, 1217 (2008). doi:10.1016/j.solmat.2008.04.012
17. C.J. Arendse, D. Knoesen, D.T. Britton, Thin Solid Films **501**, 92 (2006). doi:10.1016/j.tsf.2005.07.131
18. D. Knoesen, C. Arendse, S. Halindintwali, T. Muller, Thin Solid Films **516**, 822 (2008). doi:10.1016/j.tsf.2007.06.210
19. I. Montero, L. Galan, O. Najmi, J.M. Albella, Phys. Rev. B **50**, 4881 (1994). doi:10.1103/PhysRevB.50.4881
20. G. Lucovsky, J. Yang, S.S. Chao, J.E. Tyler, W. Czubatyi, Phys. Rev. B **28**, 3225 (1983). doi:10.1103/PhysRevB.28.3225
21. D. Han, K. Wang, J.M. Owens, J. Appl. Phys. **93**, 3776 (2003). doi:10.1063/1.1555680
22. G. Lucovsky, Z. Zing, Z. Lu, D.R. Lee, J.L. Whitten, J. Non-Cryst. Solids **182**, 90 (1995). doi:10.1016/0022-3093(94)00578-8
23. J.K. Rath, H. Meiling, R.E.I. Schropp, Jpn. J. Appl. Phys. **36**, 5436 (1997). doi:10.1143/JJAP.36.5436
24. C. Gonalves, S. Charvet, A. Zeinert, M. Clin, K. Zellama, Thin Solid Films **403–404**, 91 (2002). doi:10.1016/S0040-6090(01)01553-X
25. D. Stryahilev, F. Diehl, B. Schroeder, J. Non-Cryst. Solids **266–269**, 166 (2000). doi:10.1016/S0022-3093(99)00800-5
26. M.H. Brodsky, M. Cardona, J.J. Cuomo, Phys. Rev. B **16**, 3556 (1977). doi:10.1103/PhysRevB.16.3556
27. H. Shanks, C.J. Fang, L. Ley, M. Cardona, F.J. Desmond, S. Kalbitzer, Phys. Status Solidi B **100**, 43 (1980). doi:10.1002/pssb.2221000103
28. U. Kroll, J. Meier, A. Shah, S. Mikhailov, J. Waber, J. Appl. Phys. **80**, 4971 (1996). doi:10.1063/1.363541
29. T. Kaneko, M. Wakagi, K. Onisawa, T. Minemura, Appl. Phys. Lett. **64**, 1865 (1994). doi:10.1063/1.111781
30. Y. He, C. Yin, G. Cheng, L. Wang, X. Liu, G.Y. Hu, J. Appl. Phys. **75**, 797 (1994). doi:10.1063/1.356432
31. H.P. Klung, L.E. Alexander, *X-ray Diffraction Procedures* (Wiley, New York, 1974)
32. E. Bustarret, M.A. Hachicha, M. Brunel, Appl. Phys. Lett. **52**, 1675 (1988). doi:10.1063/1.99054
33. R. Swanepoel, J. Phys, J. Phys. E: Sci. Instrum. **16**, 1214 (1983). doi:10.1088/0022-3735/16/12/023
34. R. Swanepoel, J. Phys, J. Phys. E: Sci. Instrum. **17**, 896 (1984). doi:10.1088/0022-3735/17/10/023
35. E.C. Freeman, W. Paul, Phys. Rev. B **5**, 3017 (1972). doi:10.1103/PhysRevB.5.3017
36. S.H. Wemple, M. Didomenico, Phys. Rev. B **3**, 1338 (1971). doi:10.1103/PhysRevB.3.1338
37. M. Yamaguchi, K. Moigaki, Philos. Mag. B **79**, 387 (1999). doi:10.1080/13642819908206415